HYPER-X STAGE SEPARATION TRAJECTORY VALIDATION STUDIES

Paul V. Tartabini*, David M. Bose†, John D. McMinn*, John G. Martin‡ and Brian K. Strovers†

Abstract

An independent twelve degree-of-freedom simulation of the X-43A separation trajectory was created with the Program to Optimize Simulated trajectories (POST II). This simulation modeled the multi-body dynamics of the X-43A and its booster and included the effect of two pyrotechnically actuated pistons used to push the vehicles apart as well as aerodynamic interaction forces and moments between the two vehicles. The simulation was developed to validate trajectory studies conducted with a 14 degree-of-freedom simulation created early in the program using the Automatic Dynamic Analysis of Mechanics Systems (ADAMS) simulation software. The POST simulation was less detailed than the official ADAMS-based simulation used by the Project, but was simpler, more concise and ran faster, while providing similar results. The increase in speed provided by the POST simulation provided the Project with an alternate analysis tool. This tool was ideal for performing separation control logic trade studies that required the running of numerous Monte Carlo trajectories.

Nomenclature

α	Angle of attack, deg
β	Sideslip angle, deg
$C_{A,}$	Axial Force Coefficient
C_l	Rolling Moment Coefficient
C_{lp}	Rolling Moment Damping Derivative with respect to Roll Rate
C_{lr}	Rolling Moment Damping Derivative with respect to Yaw Rate
C_m	Pitching Moment Coefficient
C_{mq}	Pitching Moment Damping Derivative with respect to Pitch Rate
C_N	Normal Force Coefficient
C_n	Yawing Moment Coefficient
C_{np}	Yawing Moment Damping Derivative with respect to Roll Rate
C_{nr}	Yawing Moment Damping Derivative with respect to Yaw Rate
C_Y	Side Force Coefficient
c.g.	Center of Gravity, ft.
δ_{ail}	RV Aileron Deflection, deg
δ_{elev}	RV Elevator Deflection, deg
δ_{rud}	RV Rudder Deflection, deg
I_{XX}, I_{YY}, I_{ZZ}	Major Moment of Inertia, slug-ft^2
I_{XY}, I_{YZ}, I_{XZ}	Cross Product of Inertia, slug-ft^2
ϕ	Body Roll Angle, deg.
ϕ_{final}	Body Roll Angle at End of Separation, deg.
ω_n	Natural Frequency, rad/s

Introduction

In its 1999 Integrated Space Transportation Plan, NASA identified the goal of developing a third generation reusable launch vehicle (RLV) capable of delivering payloads to orbit at a cost of $100 per pound and with a probability of failure of less than one in a million by the 2025 time frame.[1] It is widely recognized that meeting such ambitious goals will require an RLV that utilizes an advanced air-breathing propulsion system capable of drastically increasing I_{SP} performance over today's all-rocket vehicles as well as providing a means for improving safety and achieving aircraft-like operations. Nu-

* NASA Langley Research Center, Member AIAA.
† Analytical Mechanics Associates, Inc, Non-Member AIAA
‡ NASA Langley Research Center, Senior Member AIAA.

merous third generation vehicle architectures have been proposed that integrate dual mode supersonic combustion ramjet (scramjet) engines into the vehicle design through either combined cycle or combination cycle modes.[2-4]

Scramjet engine development has progressed since the early 1960s through numerous ground-based testing programs.[5,6] In 1995 NASA initiated its Hyper-X program with the aim of moving scramjet research from the laboratory to the flight domain. The first research vehicle to be test flown under the Hyper-X Program will be the X-43A, which has the goal of providing the first flight data of an operational hydrogen-fueled airframe-integrated scramjet engine. Potential benefits from this initial test program include the demonstration of key scramjet technologies as well as the validation and calibration of experimental methods and computational tools employed in the design and analysis of hypersonic air-breathing vehicles.[7,8]

The X-43A research vehicle (RV) serves as the trailblazer in the Hyper-X program and is narrowly focused on the advancement of essential scramjet technologies and the building of hypersonic flight experience. To reduce cost, the vehicle was designed to be only large enough to collect seconds worth of engine data at realistic operating conditions. Thus, the vehicle must be boosted to its test conditions on the first stage of a Pegasus launch vehicle. For this boost phase of flight, the RV is mounted to an adapter connecting it to the nose of the booster. The booster/adapter configuration is called the Hyper-X Launch Vehicle (HXLV). The entire HXLV/RV stack is carried to the launch point off the coast of California by a NASA B-52 where it is dropped at an altitude of 40,000 ft and boosted due west to an altitude of roughly 95,000 ft for the Mach 7 engine test condition. At the test point the RV separates from the HXLV and performs the engine test, which results in the acquisition of nearly 10 sec. of powered scramjet flight data. The data is relayed back to ground stations and the vehicle is not recovered.

Three flights of the X-43A research vehicle were originally planned at Mach numbers of 7, 7 and 10. In June 2001, the first attempt to fly the X-43A ended in failure when the booster/research-vehicle stack veered off course and had to be destroyed. Although the cause of the mishap is still being investigated, an intense Return-to-Flight (RTF) effort has been initiated and a new Mach 7 X-43A flight is planned in late 2003. The RTF phase of the mission is focused on reducing the risk of the most critical flight segments to enhance the probability of mission success.

One of the highest risk events that will occur during the X-43A flight is the high dynamic pressure separation of the RV from the first-stage Pegasus booster (see Fig. 1). Separation of two flight vehicles at the conditions required for a successful test flight (i.e., Mach 7, dynamic pressure of 1066 psf) is unprecedented. To assess the risk associated with the stage separation, a 14 degree-of-freedom (DOF) simulation was created early in the program using the Automatic Dynamic Analysis of Mechanics Systems (ADAMS) simulation software.[9] ADAMS is a generalized, commercial code that can provide high fidelity dynamic modeling of complex mechanical systems. For this application, ADAMS modeled the multi-body 6 DOF motion of the HXLV and the RV as well as two pyrotechnically actuated pistons that will push both vehicles apart. Additional user-defined subroutines were developed to include the effects of the atmosphere, aerodynamic force and moments, piston forces, RV control system, inertial navigation system and control surface actuators. The entire simulation, which includes the user-defined modules wrapped around the ADAMS solver, is known as SepSim.

SepSim has been used extensively to understand the impact of the various system uncertainties on the stage separation event. The simulation has been run in a Monte-Carlo fashion to estimate the probability of re-contact between the two vehicles and to evaluate the capability of the X-43A control system to limit attitude excursions during separation as well as ensure a proper post-separation vehicle attitude.[10,11]

Prior to the 2001 flight, validation of the SepSim tool consisted of modular level checks performed by comparing simulation results with independent stand-alone models, and one integrated level check that compared results with those from an independent six-degree-of-freedom RV simulation. This independent simulation modeled the dynamical motion of only the RV during separation by including additional force and moment increments due to the pistons and the aerodynamic interference effects on top of the baseline aerodynamic forces predicted for free flight. Since these increments were computed by SepSim, the value of the validation was limited, providing only a check of model integration and the equations of motion.

In order to obtain a more comprehensive validation of SepSim, and thus satisfy one objective of the Return-To-Flight activity, an independent simulation of the Hyper-X stage separation was developed using the Program to Optimize Simulated Trajectories (POST)[12] to model the six degree-of-freedom motion of both flight vehicles without relying on SepSim results for input; that is, all forces and control surface commands are calculated independently. This paper documents the development and capabilities of this new 12 degree-of-freedom simulation as well as how it was used to validate the SepSim simulation and Monte Carlo analyses. Results are also presented from trade studies and sensitivity analyses that were performed with the POST simulation to verify RV control system settings and to assess different modeling assumptions.

Approach

A dimensioned drawing of the HXLV/RV stack is shown in Fig. 2 to illustrate the relative size of each vehicle and to identify the Launch Vehicle reference frame (LV frame), which is used in this paper to locate various geometric points of interest including vehicle center-of gravity locations and aerodynamic moment reference points.

The convention used to describe relative distances and orientations between the RV and HXLV is depicted in Fig. 3. Key to this convention is the separation reference point, which is fixed in the RV body frame. At the start of separation this point is coincident with the moment reference point of the HXLV (MRP_{HXLV}). As the vehicles move apart the three components of the relative position vector from the MRP_S to the MRP_{HXLV} are called X_{SEP}, Y_{SEP} and Z_{SEP}. Since these distances represent the position of the HXLV relative to the RV, X_{SEP} becomes more negative as the vehicles move apart. Similarly, a positive value of Z_{SEP} indicates that the spent HXLV is below the RV. Also specified in the figure are the 2-3-1 Euler angles, A_{SEP}, B_{SEP} and C_{SEP} that describe the orientation of the booster body frame relative to the RV body frame. These six relative quantities, along with the RV angle of attack and sideslip are used to define the aerodynamic interference database. Transition from the interference region to free flight is provided through interpolation based on X_{SEP}.

The nominal stage separation event will be initiated 10 sec after the burnout of the Pegasus solid rocket motor at an angle of attack of 0 deg, a Mach number of 7.075 and a dynamic pressure of 1066 psf. The POST simulation was started at this point with the stack still intact. Actual separation of the RV from the HXLV commences 5 ms later when the two ejector pistons mounted on the booster were fired, pushing the two vehicles apart.

Figure 4 shows a timeline of key events during the nominal separation trajectory. At ~100 ms the pistons reach the end of their 9-inch extension, and the vehicles are moving apart at roughly 16 ft/s. Between 80 and 120 msec the booster commands a 10 deg elevon deflection to induce a nose-down pitching motion, moving it further away from the separated RV as it descends uncontrolled back to Earth. For the first ~250 ms of separation the two vehicles are in close enough proximity that aerodynamic interference effects have a significant effect on the trajectory. These effects gradually diminish as the vehicles move apart and are gone by ~350 ms when the separation distance is on the order of 6 ft. By 500 msec all of the RV control system loops are closed and the vehicle begins to track angle of attack and roll angle commands. By the end of the 2.5 sec separation event, the RV is at its required attitude of $\alpha = 2.5$ deg, $\beta = \phi = 0$ deg with zero attitude rates. This point marks the beginning of the RV engine test sequence.

The independent X-43A stage separation simulation was created using a new version of the Program to Optimize Simulated Trajectories (referred to as POST II).[13] The original POST program (described in Reference 12) is a commercially available, generalized trajectory simulation and optimization code that has been widely used for 30 years to design and analyze trajectories for a range of powered and unpowered aerospace vehicles. It was developed in the early 1970's and has been continuously refined and improved since that time. POST II draws on the heritage of the original code while incorporating numerous improvements and enhancements, not the least of which is the ability to simultaneously simulate more than one vehicle. In addition, POST II provides an improved table lookup functionality that enables the use of N-dimensional, non-rectangular data tables, thus making it possible to utilize the complex, eight-dimensional stage-separation aerodynamic interference database without any major modification to the code.

These new capabilities, as well as the fact that program can be easily modified by an experienced user to include vehicle control systems and non-standard trajectory models, made POST II an appropriate choice for the construction of an independent

simulation that could validate the SepSim results and verify the numerous simulation models used to predict the flight behavior of both vehicles. Also, by utilizing software specialized for trajectory calculations, it was possible to develop a simulation that provided similar results as SepSim, but was simpler and more concise. Finally, since the POST II simulation took much less CPU time to execute than the higher fidelity SepSim, it was well suited for conducting trade studies and sensitivity analyses that required the running of numerous Monte Carlo cases, thus providing the project with an additional analysis tool.

One objective in the simulation development was to minimize changes to the POST source code. Thus, whenever possible, logic required to activate simulation events was modeled in the POST input file, which is accessible to the user and can be changed without recompiling the code. Implementing event criteria in this manner was made possible by a new POST II capability that enables multiple event criteria to be triggered using Boolean logic operators. When code changes were necessary, hard-wired parameters were avoided and a modular programming style was adopted that made it easy to upgrade or switch out simulation models. A final objective was to streamline the simulation by ignoring higher fidelity models that did not significantly affect the vehicle dynamics over the duration of the 2.5 sec. separation event. The effect of neglecting these models will be discussed later.

The development of the POST simulation was a key part of the X-43A Return-to-Flight risk mitigation strategy. The studies conducted with POST were primarily concerned with validating the ADAMS-based SepSim simulation. The initial step in the validation process was to compare nominal separation results from both simulations and to explain any differences. In order to determine if discrepancies in the results were due to the higher-order models that were neglected in the POST implementation, a version of SepSim was created that did not include these specific higher order model elements, thus allowing direct comparisons. Once traceability was established for the nominal case, POST was used to perform a validation of the SepSim Monte Carlo analysis.

Additional trade studies were performed with POST to verify different aspects of the separation control logic. POST was used for these analyses because of its speed advantage over SepSim, which enabled the screening and evaluations of many different options. When comparing these options there were three main separation objectives that were considered. First, it was important to minimize the chance of the two vehicles coming into re-contact after the pistons initiated separation. Next, the transient behavior of the vehicle had to be controlled so as to avoid large excursions in vehicle attitude without exceeding the limits on control surfaces deflections and actuator rates. Finally, there was an end-of-separation attitude target box ($2 \text{ deg} \leq \alpha \leq 3 \text{ deg}$, $-0.5 \text{ deg} \leq \beta \leq 0.5 \text{ deg}$) that, if satisfied, increased the likelihood of a successful engine test. Different metrics that provided a measure of the realization of these three objectives were considered when comparing separation trajectories. Once candidate options were identified from the POST analysis, they were implemented in SepSim, which acted as the final truth model for the Project.

Determining if and when the two vehicles came into re-contact required post-processing of the trajectory data. For high fidelity re-contact analysis the Project employed a three-dimensional modeling software toolkit called DVISE, which utilized the full geometry of both vehicles. For the studies addressed in this paper a MATLAB script was developed that could predict re-contact for simplified geometries. The script was very fast and (unlike DVISE) could also provide a measure of the closest distance between the two geometries at any point in the trajectory (called proximity). The proximity parameter was useful for making relative comparisons between two different separation trajectories, particularly when neither trajectory results in re-contact.

To utilize the script, the surfaces on the RV and adapter in contact prior to separation were approximated as two, initially coincident, convex quadrilateral planes. Re-contact occurrences were determined by moving each quadrilateral through its predicted translation and rotation and tracking the corner points and edges. The script was validated by modeling the same quadrilateral geometry with DVISE. Interestingly, it was found that the simplified geometry was conservative and tended to over-predict the occurrence of re-contacts.

Simulation Models`

In the POST II simulation, the translational and rotational equations of motion were integrated using a 4^{th} order fixed-step Runge-Kutta integrator with a time step of 0.001 sec. The time step was reduced by a factor of 10 while the piston forces were active.

This differed from SepSim, which utilized a variable-step, integration scheme capable of solving stiff problems.

The 1995 Global Reference Atmospheric Model (GRAM-95) was used to model atmospheric properties in both simulations.[14] Winds were not modeled in POST II (although they were in SepSim) since they had a small effect on the separation trajectory which occurs entirely at Mach ~7.

A brief description of some of the other more detailed simulation models required to define the complex dynamic interactions during stage separation is provided below. Unless otherwise noted, model implementation was carried out in POST in the same manner as SepSim.

Mass Properties

The nominal weight of the entire HXLV/RV stack at the initiation of stage separation is 13,576 lb with the RV alone comprising 2,738 lb of the total. The mass, center-of-gravity and inertia characteristics of both vehicles are listed in Table 1.

Aerodynamics

A complex aerodynamic database that was constructed from wind tunnel data and computational fluid dynamic calculations was employed in the stage separation flight simulation.[15-17] The database provides force and moment coefficients for three different vehicle configurations (stack, HXLV and RV) in regions of free-flight and aerodynamic interference. Also included in the database are the force/moment contributions of the HXLV control surfaces (elevons and rudder), the RV control surfaces (all-moving wing and twin vertical tails with rudder) as well as pitch, roll and yaw damping derivatives for the RV.

The interference portion of the database was constructed predominantly from wind tunnel measurements taken at the Arnold Engineering Development Center (see Ref. 16) and contains over 21,000 data points for each of the 12 aerodynamic force and moment coefficients (6 for the booster and 6 for the RV). The 8-dimensional database was parameterized with respect to α_{RV}, β_{RV}, the X_{SEP}, Y_{SEP} and Z_{SEP} separation distances and the three Euler angles describing the relative orientation of the two vehicles (A_{SEP},B_{SEP} and C_{SEP}).

The base coefficients were determined using the interference database beginning at 5 ms when the vehicles first became separated until the X_{SEP} separation distance reached -44 in. (note that X_{SEP} becomes more negative as the vehicles move apart). Once X_{SEP} exceeded -69 in., both vehicles were assumed to be out of the interference region (see Ref. 17) and the free flight databases were used exclusively. In the region between -44 and -69 inches the base coefficients were ramped linearly from the interference values to the free flight values. Note that for both vehicles the same control surface increments were used during the entire separation trajectory (i.e., the control effectiveness of the RV was not impacted by the proximity of the HXLV).

Figure 5 shows the variation of the RV pitching moment coefficient about the c.g. from the start of separation until the free flight region (roughly 0.35 sec into separation) for the nominal trajectory. The interference effect acts as a disturbance to the free flight behavior, essentially reducing the amount of nose-up pitching moment that would be present if the vehicle were in free flight. The linear fairing in the transition region is evident. The uncertainty bounds shown in the figure will be discussed in a later section.

Ejector Piston

The schematic in Fig. 6 illustrates the horizontal and vertical locations of the pyrotechnically activated ejector pistons that initiate the separation process. There are two pistons that are each positioned ~9 inches on each side of the vehicle centerline. The pistons, which emanate from the HXLV, are initially in contact with a cup-like ball joint attached to the RV that permits rotation but not translation about the piston contact point. The ends of each piston remain in contact with the RV for approximately 0.1 sec until they reach the end of their 9-in. stroke length. Note that the line-of-action of the axial piston force is 4 deg below the horizontal, which is above the RV's center-of-gravity. Consequently, the piston induces a nose-down pitching moment on the RV.

As in SepSim, each piston is modeled as a spring with the axial force determined from a test-derived force profile (see Fig. 7) and lateral restoring forces computed from beam deflection theory. Modeling the pistons in this manner avoids the need to consider constraint equations in the POST II formulation. In POST (unlike SepSim) the pistons are assumed to be massless and frictionless and only the

effect of their reaction forces is modeled. The force model is deactivated (set to zero) when the piston extension length is reached.

Guidance, Navigation and Control

Constant guidance is employed for both vehicles throughout separation. The HXLV is initially held at its trim attitude before an open-loop 10-deg elevon nose-over is initiated 0.12 sec into separation, and the RV is targeted to its required test sequence attitude. In addition, the inertial navigation system (INS) is not modeled in the POST II simulation as it was in SepSim, and thus, the true attitude and rate data were provided as inputs to the control system. Neglecting the effect of the INS simplified the overall implementation and had only a small impact on the simulation results.

The RV controller was developed in the MATLAB/Simulink environment.[18] C source code was autogenerated by MATLAB for implementation in the POST II simulation. The controller is initiated at 0.01 sec. and is called at a frequency of 100 Hz. An internal timer is started when a break-wire, which is connected to both the HXLV and RV, is broken as the pistons begin to push the vehicles apart. All important controller events are referenced to the time measured by this clock, which is referred to as T_{SEP}.

At a T_{SEP} of 1 ms an open-loop elevator command is initiated moving the wings on the RV symmetrically to a 6 deg deflection (trailing edge down). This increases the lift on the tail and reduces the risk of a re-contact. Feedback control is not employed until after a T_{SEP} of 100 ms, when the pistons are at their full extension and the RV is no longer in contact with the HXLV. For the next 200 ms both vehicles are close enough in proximity that the possibility of a re-contact remains.

To minimize the likelihood of vehicle departure, the control system first provides essential rate damping in the pitch and roll channels. Beginning at 100 ms the elevators are controlled in response to pitch rate and the ailerons in response to roll rate. In contrast, the yaw-rate to rudder loop is not closed until 400 ms. This delay alleviates a rudder rate limiting issue, uncovered early in the Monte Carlo analysis, in a trade with transient sideslip response. At 500 ms the outer loops are closed and the control system begins to regulate vehicle response to angle of attack and roll commands. Trade studies performed to verify this separation control logic will be discussed later.

Control Surface Actuators

The RV and HXLV control surface dynamics were implemented as second order linear actuator models. HXLV actuators rates were limited to 27 deg/s and RV actuator rate limits, which were dependent on the load, generally ranged between 100-120 deg/s. Surface free play, which was included in SepSim, was not modeled in the POST II simulation.

Results and Discussion

SepSim Validation

With the exception of the RV controller autocode, the entire POST simulation was developed independently of SepSim. That is, even though the models in each simulation employed the same methodology and the modeling data were derived from the same sources, new subroutines and data tables were created for use in POST and no component of SepSim (except the controller) was directly used in the POST implementation. The same controller was used in both simulations to mimic flight software; however, data sampling and command quantization were performed independently in POST.

The process of constructing an independent simulation provided a comprehensive check of nearly all the models implemented in SepSim. This proved invaluable when discrepancies detected between the two sets of results led to the discovery of two minor errors in SepSim. Once both simulations were finalized, an initial comparison was made of the nominal case.

For the nominal trajectory the angle of sideslip and roll angle for the RV remain at zero degrees throughout separation. The angle of attack and elevator deflection profiles computed by POST and SepSim are shown in Figs. 8 and 9, respectively. There is an initial nose-down rotation in the first 0.2 sec. due to a combination of piston forces and aerodynamic interference. However, as pitch rate feedback begins to arrest this initial nose-down moment and the RV transits out of the interference region, the vehicle begins to nose-up toward the final desired angle of attack of 2.5 degrees.

There is a noticeable difference in the angle of attack profiles determined by each simulation even

though both are similar and have a final angle of attack that is well within the desired target box. In particular, the POST results overshoot SepSim by nearly 0.25 deg. In Fig. 9 the differences in the elevator deflection profiles near 2.5 sec indicated that each simulation was targeting a slightly different trim attitude, most likely due to INS misalignment errors that were modeled in SepSim but not POST. When a modified version of SepSim was created that made many of the same modeling assumptions as POST, the agreement between the simulations improved significantly and the profiles nearly laid on top of each other. Similar results are also seen in Fig. 10, which shows the proximity parameter as a function of X_{SEP}. Once again the small differences between the simulations were eliminated when the modified version of SepSim was used for the comparison.

To establish traceability between POST and SepSim, results were obtained from several different versions of SepSim that had varying degrees of model fidelity. By comparing these results with those from POST it was found that discrepancies in attitude profiles were almost entirely due to two models that were not implemented in POST: free play in the actuators and the inertial navigation system. This fact is illustrated in Figs. 11 and 12, which compare alpha and beta profiles from POST with those from three different versions of SepSim (full version, no free play, no free play and no navigation errors). The figures show that when free play and navigation errors were removed, there was excellent agreement between the POST and SepSim results. Removing free play tended to improve agreement in the first part of the trajectory profiles, while removing navigation errors tended to improve it near the end. For the case shown, the difference between the POST and modified SepSim (without free play and navigation errors) profiles was less than 0.04 deg in alpha and 0.02 deg in beta. Similar agreement is seen in the control surface deflection time histories shown in Fig. 13.

As long as the traceability between the simulations was established, it was not necessary to modify POST to include free play and an INS since their implementation in SepSim could be verified adequately through comparison with standalone tools. Moreover, even though there were differences in the attitude profiles predicted by POST and SepSim, the differences were small and there was still good agreement between the parameters of interest (e.g., final alpha and beta, peak attitude and attitude rates, re-contact occurrence, etc.). Thus, results from POST were adequate for conducting trade studies, especially since most of the studies were primarily concerned with the relative differences (i.e., deltas) between trajectories.

A final note is made regarding the effect of the massless and frictionless piston model implemented in POST. Figure 14 compares the lateral piston force (in the Y_{LV} direction) profile computed by POST and SepSim. In both simulations the lateral force became smaller as the piston extended and the effective piston length increased until eventually the restoring force was not large enough to bring the lateral deflection back to zero. This point was reached sooner for the SepSim case, which accounts for the mass of the piston and constrains the piston motion relative to the booster using a translational joint. Also, the undamped force computed by POST oscillated about the SepSim value. Consequently, the attitude profiles of both cases (see. Figs. 11 and 12) are nearly identical in the first 0.2 sec, confirming previous SepSim studies that suggested neglecting the mass and friction of the pistons would not have a significant impact on the simulation results.[19]

Monte Carlo Analysis

To account for modeling uncertainties, Monte Carlo analyses were performed on the trajectory to determine statistical estimates of the separation metrics. In a typical POST analysis 1200 different simulations were run with randomly perturbed values of over 90 different modeling parameters. Initial condition dispersions and mass property uncertainties are listed in Tables 2 and 3 along with their corresponding 3-σ variance (normal distribution) or min/max range (uniform distribution). The aerodynamic uncertainties, which were uncorrelated, consisted of multipliers that were applied to the RV base coefficients and damping derivatives in the free flight regime and increments that were added to the base coefficients of both vehicles in the region of aerodynamic interference. These increments accounted for measurement uncertainties from the separation wind tunnel tests and errors due to database interpolation.[20] The 3-σ values of both the free flight multipliers and interference increments are listed in Table 4. Note that the interference increments were dependent upon the horizontal separation distance, X_{SEP}. All of the aerodynamic uncertainties were sampled from a Normal distribution except for the free flight aerodynamics which utilized a uniform distribution.

To verify the SepSim Monte Carlo procedure 200 cases were run with POST and both the full and modified versions of SepSim, with the same uncertainties applied in each simulation. Table 5 shows a comparison of some of the result statistics. Overall there was good agreement between the POST and SepSim statistics, especially when the modified version (without free play or navigation errors) was used. The number of failed cases, which were defined as ones that either diverged or had peak values of alpha or beta greater than ± 10 degrees, was roughly the same for each simulation. Also, slightly more cases were predicted to fall outside the target box with the full version of SepSim, due to the effect of INS errors. The agreement between POST and the modified version of SepSim is further illustrated in Fig. 15, which shows the mean, 1 and 99-percentile angle of attack values at each time step for all of the 200 Monte Carlo cases computed by both simulations.

One additional note should be made about the difference in the time required to run Monte Carlo analyses with POST and SepSim. First, individual trajectories could be run faster in POST due to differences in formulation, most notably the integration scheme. In addition, it was possible to implement POST in a parallel processing mode so that as many cases as available processors could be run simultaneously. This parallel processing capability was available with SepSim as well but was limited due to license restrictions. Consequently, to run these 200 comparison cases took nearly 13 hours with SepSim using 4 processors while the analysis was completed on 16 processors in roughly 30 minutes with POST.

Control System Logic Verification

Two studies were conducted using POST to verify some aspects of the RV control system logic. These analyses were well suited for POST since they required the running of numerous Monte Carlo cases.

The first of the studies investigated the method of fading in the yaw rate feedback loop for rudder control. In the current strategy the rudder is held at zero deflection after the break wire snaps until the feedback loop begins to fade in 400 ms later over a duration of 600 ms. That is, full rudder feedback control is not active until ~1 sec. after separation commences. This approach differs from the one used in controlling the wings in which full pitch and roll rate feedback control begins 100 msec after break wire when the RV clears the pistons. The purpose of delaying rudder control is to improve off-nominal performance by avoiding large surface deflections and actuator rates induced by aerodynamic interference effects during the first 350 ms of separation. The delay permits the natural stability of the RV to reject sideslip before the controller is engaged. This effect is demonstrated in Figs. 16 and 17, which shows representative beta and rudder rate profiles obtained using the baseline 400/1000 ms fade strategy and one that mimicked the strategy used for the wings with feedback control being stepped in at 100 ms. (100/100). The positive and negative peak transient beta excursions are increased by 0.5 degrees by fading rather than stepping in the feedback control (see Fig. 16). This reduction, however, came at the expense of much higher rudder actuator rates. Figure 17 shows that for the 100/100 case the rudder rate immediately exceeds 110 deg/s and then quickly reverses to –100 deg/s before beginning to settle out. By contrast, implementing a 400/1000 fade keeps the rudder rate below 40 deg/s for the entire trajectory.

POST was used to determine if the 400/1000 ms fade provided the best performance from a statistical perspective. Figure 18 shows a time plot of five different loop closure options that were considered. In addition to the baseline 400/1000 and 100/100 cases discussed previously, three additional fade-in cases were evaluated: 100/1000, 200/800 and 300/1500. To perform these studies 1200 POST Monte Carlo cases were run for each of these options with the same 1200 sets of dispersions. The number of failures and cases outside the target box were not significantly affected by the yaw fade parameters. As expected, the largest effect was on the rudder rate limit and transient beta characteristics. These results are summarized in Table 6 where, for each loop closure option, the percent of cases with beta exceeding ±4 deg and rudder rate exceeding ±80 deg/s is shown. Once again, the need to have some type of fade-in strategy is evident by considering the 100/100 results in which nearly half the cases had rudder rate limits greater than 80 deg/s. In general, the results illustrate the trade between minimizing beta excursions and keeping rudder rates low. If both criteria are equally weighted, the 300/1500 strategy does the best job; however, by delaying full rudder feedback until 1500 ms after separation, roll performance begins to degrade. When the percentage of cases with a final roll angle outside ± 10 degrees was considered as an additional criterion, the 400/1000 strategy was superior.

Further insight is gained by examining Fig. 19, which shows colored contours depicting the peak

beta value for a representative off-nominal trajectory run at a range of different fade-start/fade-duration values across the trade space. Also shown on the plot are contour lines of the peak rudder rate. Symbols denote the cases used in the Monte Carlo analysis. The figure illustrates that beta excursions are not very sensitive to increasing the duration of the fade. Increasing the fade duration also has diminishing returns with respect to reducing rudder rates. The figure shows that the baseline 400/1000 case is positioned in an area with high rudder-rate contour gradients, and thus is able to keep rates low without much of a penalty in peak beta.

An additional verification study was performed to evaluate the separation elevator scheduling logic used in the RV controller. Immediately after break wire the controller issues an open-loop elevator command to bias the wings to a positive (trailing edge down) deflection before the pitch and roll rate feedback loops are closed 100 ms later. The purpose of biasing the elevator deflection is to increase the lift on the aft end of the RV as it moves off the pistons, thus reducing the likelihood of re-contact. Adjusting the elevator bias also affects the transient attitude behavior of the vehicle and the wing actuator rates. Therefore, a trade study was performed to determine if the trajectory performance could be improved by changing the elevator scheduling.

The current baseline strategy uses a 6-degree elevator bias. Additional bias settings ranging from 0 to 10 deg were evaluated in separate 400-case Monte Carlo analyses. To add conservatism, larger aerodynamic interference uncertainty increments were used. Comparisons were based on the ability to hit the $\alpha-\beta$ target box, transient attitude performance, control surface rates and proximity metrics. The results are shown in Table 7.

As expected, when the bias was increased, the number of cases with a minimum proximity of less than one inch at X_{SEP} values between –20 and –44 in. (the region where re-contact was of greatest concern) is reduced. Note also that at low and high bias settings the wing actuator rates tended to increase. The mid-range bias settings had lower actuator rates because the elevator was biased closer to the midpoint between the position required for aerodynamic trim in the interference ($\delta_{elev} \approx 0$ deg) and free ($\delta_{elev} \approx 7$ deg) regions of flight. The trends in proximity and actuator rates are shown graphically in Fig. 20. It can be seen that increasing the bias setting beyond the baseline value of 6 deg would provide only a minimal reduction in the proximity metric (which was already low) and would lead to higher wing actuator rates. These results confirmed that the bias was set at a reasonable value and not much would be gained by adjusting it further.

Conclusions

An independent simulation was developed to validate the Hyper-X stage separation trajectory analysis using the Program to Optimize Simulated Trajectories (POST II). The POST simulation was less detailed than the official ADAMS-based simulation used by the Project, but was simpler, more concise and ran faster, while providing similar results. The POST implementation included completely independent versions of all important separation models except the RV controller, which is based on the flight software. The effect of actuator free play and navigation sensor errors were not modeled in POST since they did not have a large effect on the trajectory and were well understood models that had been validated adequately with stand alone tools. When these two effects were taken out of SepSim, the angle of attack and sideslip profiles predicted by the two simulations agreed to within 0.05 deg. Similar agreement was obtained for off-nominal cases, and statistical results from Monte Carlo analyses conducted with each simulation matched closely as well.

The rapid Monte Carlo capability provided by the POST simulation made it an ideal tool for conducting trade studies and sensitivity analyses that required the running of numerous trajectories. This capability was applied in a series of studies undertaken to verify the separation control logic. POST Monte Carlo results supported the strategy of fading in yaw-rate to rudder feedback control from 400 to 1000 ms after the start of separation to decrease the probability of high rudder actuator rates. In addition, the baseline elevator scheduling logic was shown to be adequate, and changing it attained only minimal improvements.

Acknowledgments

The authors would like to thank Melissa Ashe for her hard work in preparing this manuscript for publication. Special thanks is also extended to Anne Costa and Kurt Severence for creating some of the graphics that were used and to John Aguirre and Matt Toniolo for their help in compiling, debugging and running POST II and SepSim.

References

1 Anderson, D. M., "NASA's Integrated Space Transportation Plan," AIAA Paper 2000-3828, July 2000.

2 Hunt, J.L., and Eiswirth, E.A., "NASA's Dual-Fuel Airbreathing Hypersonic Vehicle Study," AIAA Paper 96-4591, November 1996.

3 Robinson, J.S., Culver, G.A., and Bishop, E.D., "Life Cycle Analysis of a Single Stage to Orbit (SSTO) Reusable Launch Vehicle," AIAA Paper 2003-5264, July 2003.

4 Escher, W.J.D, "On the Airbreathing/Rocket Propulsion Relationship: For Advanced Spaceflight Systems, It's the Combination that Counts," AIAA Paper 2003-5266, July 2003.

5 Andrews, E. H., "Scramjet Development and Testing in the United States," AIAA Paper 2001-1927, April 2001.

6 Cockrell, C. E., Auslender, A. H., Guy, R. W., McClinton, C. R. and Welch, S. S., "Technology Roadmap for Dual-Mode Scramjet Propulsion to Support Space-Access Vision Vehicle Development," AIAA Paper 2002-5188, October 2002.

7 McClinton, C. R., Rausch, V. L, Sitz, J. and Reukauf, P., "Hyper-X Program Status," AIAA Paper 2001-0828, January 2001.

8 Rausch, V. L., McClinton, C. R. and Hicks, J. W., "NASA Scramjet Flights to Breathe New Life into Hypersonics," Aerospace America, July 1997.

9 Anon.: Using ADAMS/Solver. Users Guide, Vol. 9.0.1, Mechanical Dynamics, Inc.

10 Reubush, D. E., "Hyper-X Stage Separation – Background and Status," AIAA Paper 99-4818, November 1999.

11 Reubush, D. E., Martin, J. G., Robinson, J. S., Bose, D. M. and Strovers, B. K., "Hyper-X Stage Separation – Simulation Development and Results," AIAA Paper 2001-1802, April 2001.

12 Brauer, G. L., Cornick, D. E. and Stevenson, R., "Capabilities and Appplications of the Program to Optimize Simulated Trajectories (POST)," NASA CR-2770, Feb. 1977.

13 Powell, R.W., et. al., "Program To Optimize Simulated Trajectories (POST II) Utilization Manual, Version 1.1.7," July 2002.

14 Justus, C.G., Jeffries, W.R., Yung, S.P., and Johnson, D.L., "The NASA/MSFC Global Reference Atmospheric Model – 1995 Version (GRAM-95)," NASA TM-4715, August 1995.

15 Engelund, W.C., Holland, S.D., Cockrell, C.E. and Bittner, R.D., "Aerodynamic Database Development for the Hyper-X Airframe-Integrated Scramjet Propulsion Experiments," *Journal of Spacecraft and Rockets*, Vol. 38, No. 6, 2001, pp. 803-810.

16 Woods, W.C., Holland, S.D., and DiFulvio, M., "Hyper-X Stage Separation Wind-Tunnel Test Program," *Journal of Spacecraft and Rockets*, Vol. 38, No. 6, 2001, pp. 811-819.

17 Buning, P.G., Wong, T.-C., Dilley, A.D. and Pao, J.L., "Computational Fluid Dynamics Prediction of Hyper-X Stage Separation Aerodynamics," *Journal of Spacecraft and Rockets*, Vol. 38, No. 6, 2001, pp. 820-827.

18 Davidson, J. et al., "Flight Control Laws for NASA's Hyper-X Research Vehicle," AIAA Paper 99-4124, August 1999.

19 Bose, D.M., "Equations of Motion for End to End Simulation," AMA Report 03-26, November 2001.

20 Bowersox, R.D., "Uncertainty Analysis of the Mach 6.0 Hyper-X Free Flyer and Booster Separation Wind Tunnel Data," Hyper-X Program Office HX-703, SSD-00-07, Nov. 2000.

HXLV	
Mass, slugs	336.84
Center of gravity, ft	
Along X_{LV} axis	25.75
Along Y_{LV} axis	0.00
Along Z_{LV} axis	-0.29
I_{XX}, slug-ft^2	3690.
I_{YY}, slug_ft^2	72821
I_{ZZ}, slug-ft^2	73403
I_{XY}, slug-ft^2	21
I_{XZ}, slug-ft^2	364
I_{YZ}, slug-ft^2	1

X43-A Research Vehicle	
Mass, slugs	85.1
Center of gravity, ft	
Along X_{LV} axis	45.07
Along Y_{LV} axis	0.00
Along Z_{LV} axis	-0.24
I_{XX}, slug-ft^2	55
I_{YY}, slug_ft^2	802
I_{ZZ}, slug-ft^2	813
I_{XY}, slug-ft^2	0
I_{XZ}, slug-ft^2	-25
I_{YZ}, slug-ft^2	0

Table 1. Nominal Mass Properties of HXLV and X-43A RV.

Initial Conditions		
Dispersions	***Mean***	***±3-σ***
Initial dynamic pressure, psf	1066	210
Stack Mach number	7.075	0.375
Stack flight path angle, deg	2.0	1.0
Stack angle-of-attack, α deg	0.0	1.5
Stack angle-of-sideslip, β deg	0.0	1.0
Stack roll angle ϕ, deg	0.0	15.0
Stack roll rate, deg/s	0.0	6.0
Stack pitch & yaw rate, deg/s	0.22	3.0

Table 2. Initial Condition Dispersions.

Mass Properties	
Uncertainty	***±3-σ or Min/Max***
HXLV	
Mass, slugs	±1.62
c.g. along X_{LV}, ft	±0.0775
c.g. along Y_{LV}, ft	±0.0225
c.g. along Z_{LV}, ft	±0.0225
I_{XX}, slug-ft^2	±166
I_{YY}, slug_ft^2	±1311
I_{ZZ}, slug-ft^2	±1321
X43-A Research Vehicle	
Mass, slugs	84.85 /85.35
c.g. along X_{LV}, ft	5.7532 /5.7698
c.g. along Y_{LV}, ft	±0.0083
c.g. along Z_{LV}, ft	-0.0400 /0.0058
I_{XX}, slug-ft^2	52 /58
I_{YY}, slug_ft^2	754 /850
I_{ZZ}, slug-ft^2	764 /862
I_{XZ}, slug-ft^2	-30/-20

Table 3. Mass Property Uncertainties for HXLV and RV Used in Monte Carlo Analysis.

Uncertainty	*±3-σ or Min/Max*
Free Flight Uncertainty Multipliers	
C_A	0.76/1.24
C_Y	0.79/1.21
C_N	0.82/1.18
C_m	0.82/1.18
C_l, C_n	0.79/1.21
Damping Derivative Multipliers	
C_{mq}	1 ± 0.60
C_{lp}, C_{nr}	1 ± 0.75
C_{lr}, C_{np}	1 ± 0.90

Interference Aerodynamic Coefficient Uncertainty Increments

RV

X_{sep}	C_A	C_Y	C_N	C_l	C_m	C_n
-4	0.0082	0.0066	0.0144	0.0063	0.0076	0.0068
-9	0.0028	0.0070	0.0085	0.0024	0.0033	0.0032
-20	0.0045	0.0027	0.0099	0.0026	0.0035	0.0026
-44	0.0010	0.0009	0.0061	0.0005	0.0011	0.0006

HXLV

X_{sep}	C_A	C_Y	C_N	C_l	C_m	C_n
-4	0.0073	0.0136	0.0109	0.0067	0.0110	0.0066
-9	0.0035	0.0133	0.0088	0.0020	0.0067	0.0032
-20	0.0073	0.0062	0.0084	0.0031	0.0049	0.0028
-44	0.0027	0.0092	0.0078	0.0019	0.0036	0.0022

Table 4. RV and HXLV Aerodynamic Uncertainties.

	SepSim	Modified SepSim	POST II
Failed Cases	3	2	2
Cases outside α-β target box	4	2	2
Avg Min/Max α, deg	-1.22/2.69	-1.16/2.78	-1.18/2.77
Avg Min/Max β, deg	-0.51/0.70	0.50/0.64	-0.51/0.66
Avg Min/Max ϕ, deg	-10.62/8.06	-9.75/7.55	-10.18/7.84
Cases with wing actuator rates > 100 deg/s	53	51	40
Cases with rudder actuator rates > 100 deg/s	2	0	0
Average minimum proximity past Xsep = -20”	1.70”	1.66”	1.65”

Table 5. Comparison of results from 200 Off Nominal Cases between POST, SepSim and Modified Sepsim (no actuator free play and sensor errors).

Case	Peak β >±4º	Rudder Rate >± 80º/s	ϕ_{final} > ±10º
400/1000 (Baseline)	1.8%	1.4%	16.3%
100/100 (No Fade)	0.3%	48.7%	15.0%
100/1000	1.4%	2.6%	15.6%
200/800	1.5%	3.1%	15.6%
300/1500	1.8%	0.7%	18.1%

Table 6. Results from Yaw Rate Loop Closure Trade Study.

Bias	2	4	6	7	8	10
% outside α-β target-box	0.5	0.3	0.3	0.0	0.0	0.3
Average Min α, deg	-0.7	-1.0	-1.4	-1.6	-1.8	-2.5
Average Max α, deg	4.9	3.5	2.9	2.8	2.7	2.7
Wing actuator rates > ± 100 deg/s	58.2	15.4	17.1	17.4	19.9	47.0
% with Minimum proximity < 1”	16.1	7.3	3.9	2.3	1.8	1.0

Table 7. Effect of Elevator Bias Setting on Key Separation Parameters.

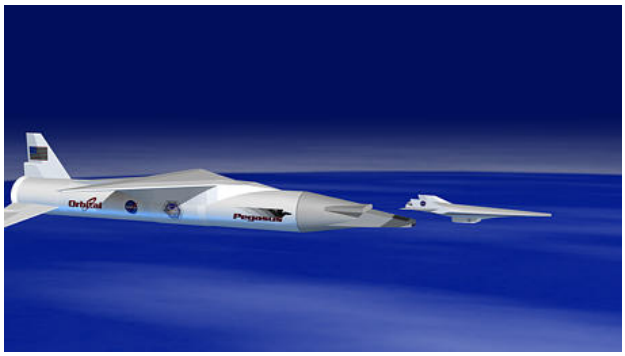

Figure 1. Artist's Conception of X-43A Separation from Pegasus Booster.

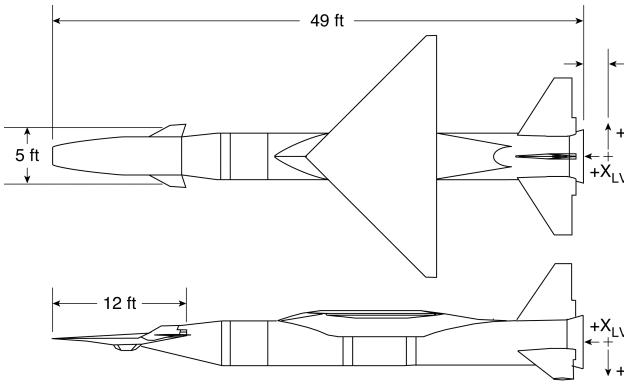

Figure 2. Hyper-X Launch Vehicle/Research Vehicle Stack.

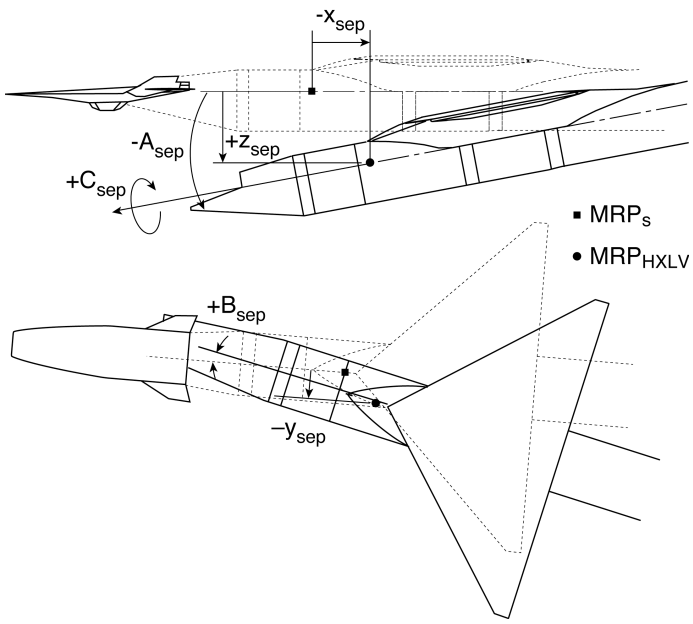

Figure 3. Hyper-X Launch Vehicle/Research Vehicle Relative Distance and Orientation Convention.

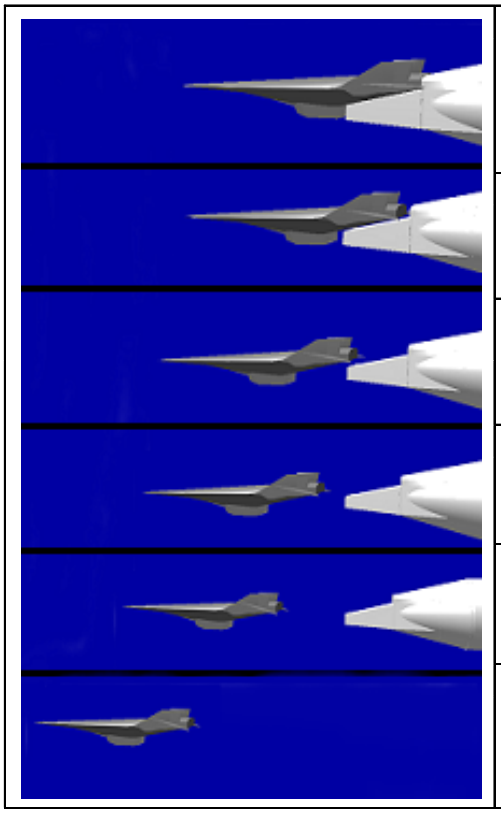

0 msec	Start of Separation Mach = 7.075 Dynamic Pressure= 1066psf $\alpha = \beta = \phi = 0^o$
100 msec	End of Piston push, * Pistons at end of 9" extension * Pitch and Yaw rate feedback loops closed * HXLV elevons to 10^o at 120 msec
250 msec	Beginning Transition from interference to free flight x_{sep} = -44"
350 msec	Free Flight x_{sep} = -69"
500 msec	All feedback control loops closed
2500msec	Start of engine test sequence $\alpha = 2.5°, \beta = 0°, \phi = 0°$

Figure 4. Nominal Separation Trajectory Timeline

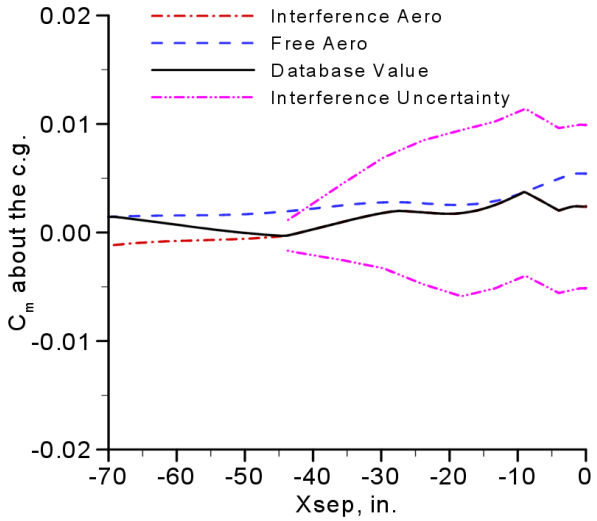

Figure 5. Interference and Free Flight Pitching Moment Coefficient with respect to X_{SEP} for Nominal Separation Trajectory.

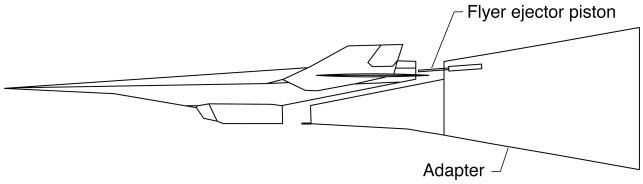

Figure 6. Horizontal and Vertical location of Ejector Pistons.

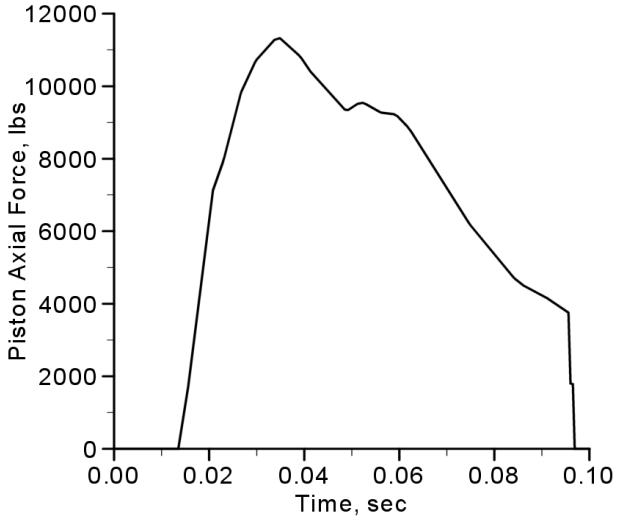

Figure 7. Nominal Piston Axial Force Profile.

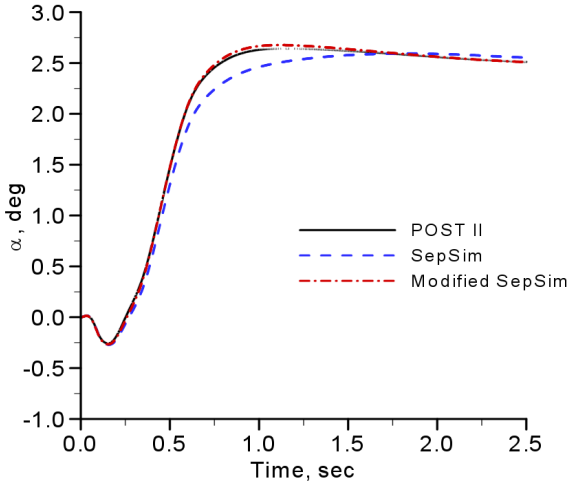

Figure 8. Nominal RV Angle of Attack Profile Comparison.

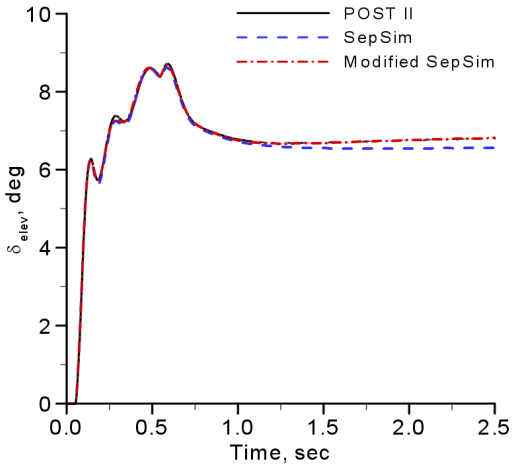

Figure 9. Nominal RV Elevator Deflection Profile Comparison.

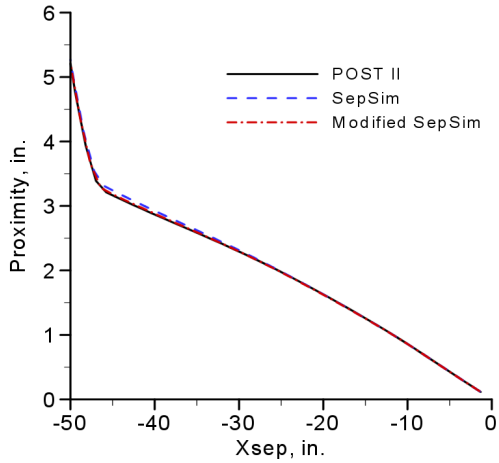

Figure 10. Proximity between RV and HXLV for Nominal Trajectory as a Function of X_{SEP}.

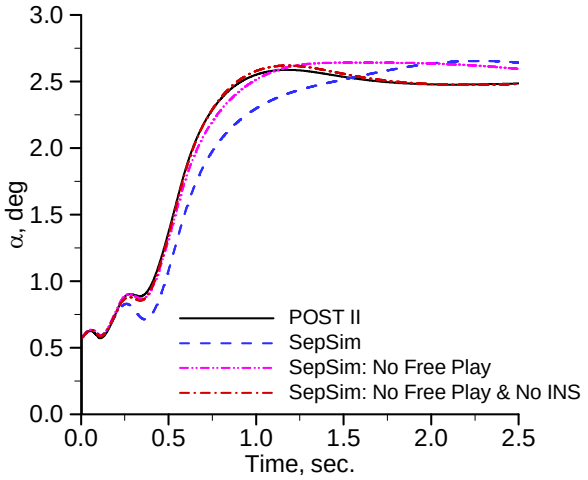

Figure 11. Angle of Attack Profile Comparison for Representative Off-Nominal Case.

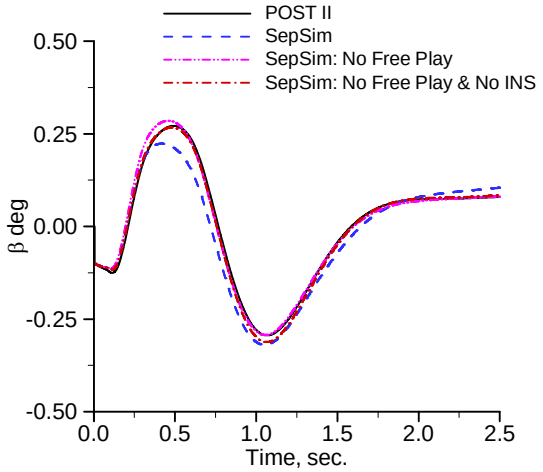

Figure 12. Angle of Sideslip Profile Comparison for Representative Off-Nominal Case.

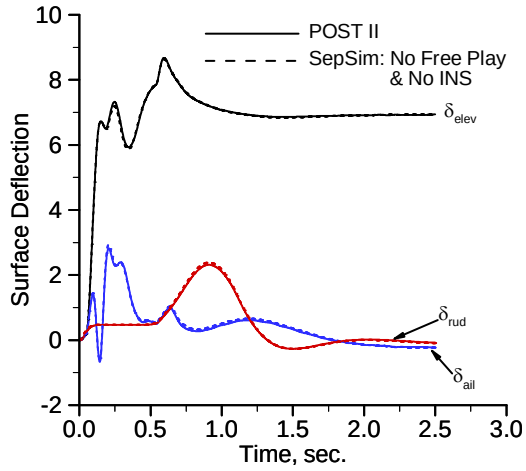

Figure 13. Control Surface Deflection Time Histories For Representative Off-Nominal Case.

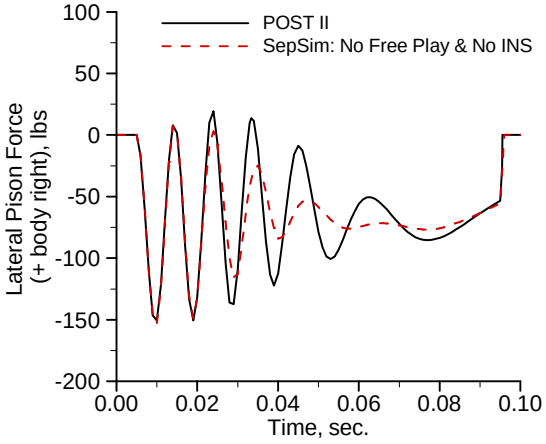

Figure 14. Lateral Piston Force Profile Comparison.

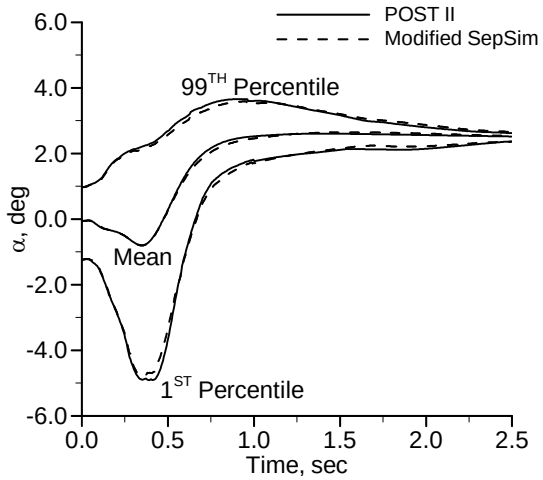

Figure 15. Comparison of Angle of Attack Profile Statistics from 200 Off-Nominal Cases.

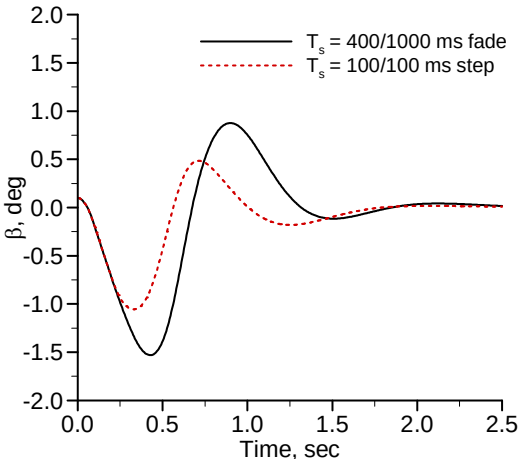

Figure 16. Effect of Fading in Yaw Rate to Rudder Feedback Loop on Sideslip Response.

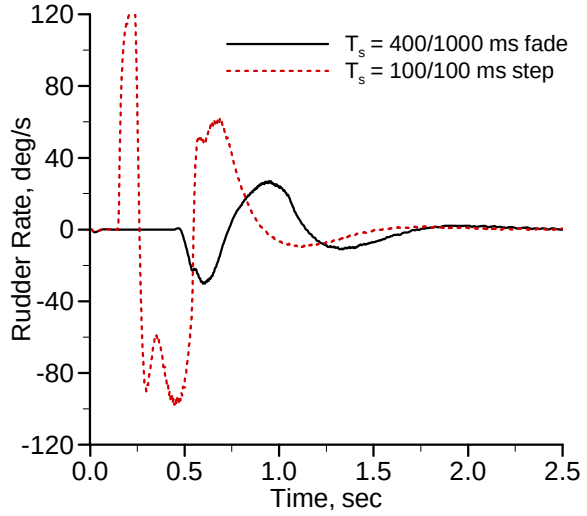

Figure 17 Effect of Fading In Yaw Rate to Rudder Feedbak Loop on Rudder Rate.

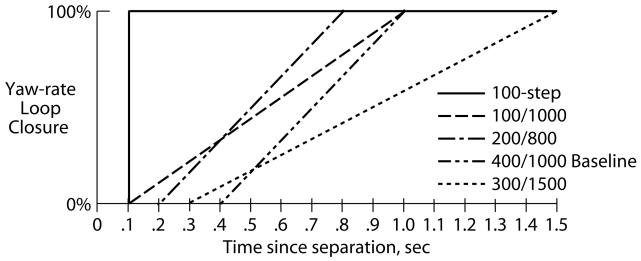

Figure 17. Yaw-rate Loop Fade-in Options.

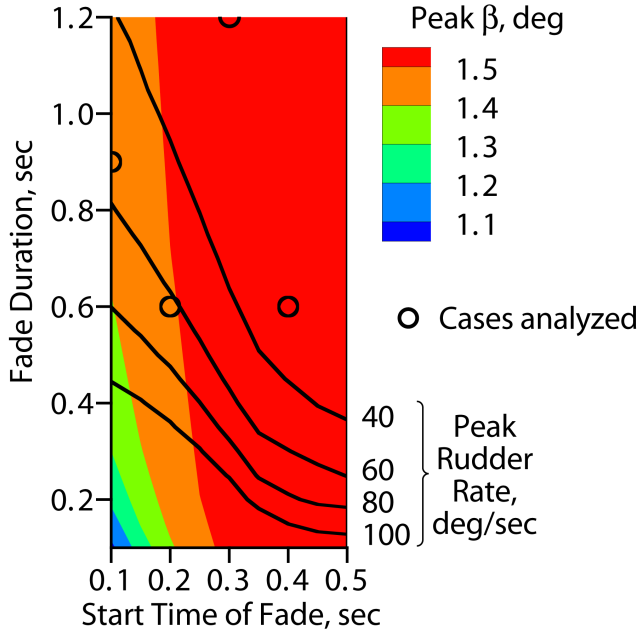

Figure 18. Effect of Fade Start and Duration on Peak Sideslip and Peak Rudder Rate.

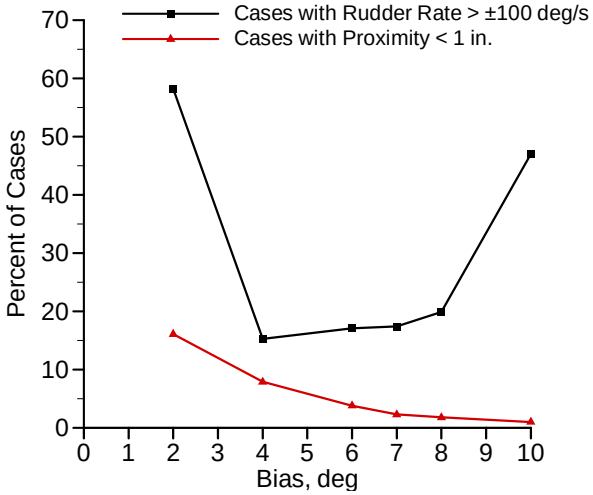

Figure 19. Effect of Elevator Bias Setting on Proximity and Peak Rudder Rate.